Lidar Measurements of Cloud-tracked Winds

SHIV R. PAL, IRINA PRIBLUDA, AND ALLAN I. CARSWELL

Institute for Space and Terrestrial Science and Department of Physics and Astronomy, York University, North York, Ontario, Canada

(Manuscript received 8 March 1993, in final form 20 July 1993)

ABSTRACT

This paper describes wind measurements derived from displacements of small-scale cloud features obtained from time-lapse videography and simultaneous lidar measurements. Lidar provides the altitude of the cloud feature with a high degree of accuracy. The video picture provides the information on the horizontal displacement coordinates of the wind speed and direction. Analysis of a large body of data has shown that the method can provide wind information with good spatial and temporal resolution. Comparisons with rawinsonde measurements show very good agreement.

1. Introduction

The purpose of the Experimental Cloud Lidar Pilot Study (ECLIPS) program (Platt 1988) is to observe clouds from below with ground-based lidars while the same cloud systems are being observed from above during overpasses of the *NOAA-10* and *NOAA-11* satellites. The main goal of this pilot study is to determine the extent to which lidar information can complement and enhance the value of the satellite data.

ECLIPS has involved the participation of about a dozen lidar groups around the world (Platt et al. 1993). To date these groups have participated in two intensive measurement campaigns. The first was in the fall of 1989 and the second in the summer of 1991. During these periods all of the groups made lidar measurements of clouds simultaneous with the overpass of the satellites. These lidar data have been collected and analyzed according to a uniform protocol and have been archived by the lidar group at NASA/Langley (contact: Dr. M. P. McCormick).

As part of this study the use of lidar to improve the derivation of winds by the tracking of cloud motions was investigated. Wind measurements by cloud tracking have been in use with satellite imagery since the 1960s, and extensive evaluations have shown the method to provide information comparable in quality to rawinsonde measurements (Leese et al. 1971; Chatters and Suomi 1975; Fujita et al. 1975; Suchman and Martin 1976; Hasler et al. 1977; Menzel et al. 1983; Sadler and Kilonsky 1985; Rutledge et al. 1991; Merrill et al. 1991 and the references therein).

Currently the major limitation of this wind measurement method is the difficulty encountered in accurately assigning the correct cloud heights. Several methods of height determination have been developed over the years, with the most common involving the use of satellite-derived cloud-top brightness temperature. This is correlated with in situ temperature profile information, if available, or with a climatological profile if no other measured data are available (Fritz and Winston 1962; Mosher 1976; Reynolds and Vonder Harr 1977; Hasler 1981).

Thin clouds, which are the most suitable tracers of the atmospheric flow at a single layer, are especially difficult to deal with since their emissivity is less than unity by some unknown and variable amount. As a result, the brightness temperature of these clouds cannot be used to determine their actual temperature. Hence, to work with this information for cloud-height assignment, one generally must apply empirical corrections or subjective operator interaction.

This error in height assignment is currently a major limitation even with the incorporation of the improved two-channel method of CO_2 slicing (Hasler et al. 1977; Bowen et al. 1979; Menzel et al. 1983; Merrill 1989; Merrill et al. 1991). Since only two channels and a simple radiative model are used, difficulties still arise, particularly with multiple cloud layers where tracer selection and recognition is not easy.

Lidar measurements have as one of their most useful features the capability of very high spatial and temporal resolution. With lidars it is possible to locate and profile cloud geometric extent to within a few meters, if desired. The measurements are limited only by the ability of the lidar pulse to penetrate the cloud. Lidar signal penetration is limited to no more than a few hundred meters in the very dense low-level and cumulus clouds, but in thin clouds, including high-level cirrus, the pen-

Corresponding author address: Prof. Allan I. Carswell, Department of Physics and Astronomy, York University, 4700 Keele Street, North York, Ontario, Canada, M3J 1P3.

etration is complete. With lidar it is possible to detect and quantitatively profile subvisual clouds that are not readily observed by satellite imagery. In fact, lidar remote wind sensing can even be done in clear air using the atmospheric aerosol as a tracer. Such work is described by Piironen and Eloranta (1993) using correlation between moving aerosol irregularities.

Thus, one goal of the ECLIPS program is to utilize the existing dataset to assess the improvements available from coupled lidar–satellite wind studies. This comparison has not yet been undertaken by any of the ECLIPS collaborators. Our group at ISTS (Institute for Space and Terrestrial Science) has taken a preliminary step in which lidar data are utilized along with ground-based time-lapse video imagery to determine winds using the same cloud-tracking approach. In this paper the results of this investigation are described.

2. Description of the method

For this work a Rayleigh–Mie (elastic backscattering) lidar (Carswell et al. 1991) has been employed. This lidar uses a Nd:YAG laser transmitter operating at both 1064 and 532 nm with a pulse repetition rate of 20 Hz. It is a fixed, vertically pointing system with a receiver having dual-polarization measurement capabilities at both wavelengths. The signals backscattered from the atmosphere can be processed by either photon counting or high-speed A/D (analog to digital) converters. Line-of-sight spatial resolution of the lidar can be as good as 3 m if desired.

Typically, the lidar fires continuously during a 3-h period centered on the satellite overpass time. The returns are hardware averaged for a 15-s interval (300 shots) then captured and stored by the data system (a dedicated PC coupled by means of Ethernet to a SUN system).

Coaligned with the lidar beam is a wide (40°) field of view (FOV) color video camera coupled to a time-lapse recorder and a video display screen. The location of the lidar beam within the camera FOV is known. At a fixed distance from the camera (at the location of the roof hatch enclosing the lidar laboratory) there is a calibration grid of known spacing and compass orientation. This provides an angular calibration of the camera FOV and allows accurate measurements of horizontal distance to be made at the cloud level once the lidar-determined distance to the cloud is established.

This arrangement permits cloud velocities (speed and direction) to be determined independent of any other input. Thus the ISTS lidar system is not only capable of eventually providing cloud-height data for the satellite wind measurements but also is a stand-alone cloud wind measurement system.

In a typical measurement run the camera records the cloud image continuously, while the lidar measures and records the return signals. Although the lidar is capable of detecting returns from altitudes up to about 90 km, for the cloud studies the observations were typically restricted to below about 15 km. An automated processing algorithm (Pal et al. 1992) is used to locate the altitude of cloud base and provide a time history throughout the observation period.

After the completed run, the videotape is processed by an operator to determine the direction and speed of the cloud movement. At present this is done manually since we do not have available to us any of the equipment for automated image analysis. In any operational version of this system all of the same image analysis methods currently being used for the satellite data could be applied (Leese et al. 1971; Smith 1975; Bowen et al. 1979; Turner and Warren 1989; Schmetz 1991).

As a cloud moves across the camera FOV, any specific cloud feature will move across the video screen along a line determined by the wind vector. The location coordinates of the feature on the screen can be determined at any time. Using the cloud height derived from the lidar profile and the calibrated camera FOV, it is then possible to translate these screen coordinates into coordinates of the feature at the location of the cloud. By taking a series of spatially separated coordinates at a sequence of times, it is possible to derive the wind speed and direction.

Typically for a low cloud at an altitude of 2 km with a wind velocity of 10 m s^{-1}, the transit time of a cloud feature across the camera FOV is about 2 min. This time increases to about 7 min for a feature in a cirrus cloud at 12 km moving with a velocity of 20 m s^{-1}. The observations have shown that during such time intervals most cloud features retain their geometric identities sufficiently to permit unambiguous tracking on the screen. There is difficulty in some rapidly evolving clouds and in these situations shorter time values were chosen. The features tracked are those that pass near the zenith direction where the lidar determines the height. Usually only the central ten degrees of the camera FOV is used. Because of the continuous video record, however, it is possible to use many sequential transit-time measurements on the same cloud to improve the accuracy of the measurement. There are some cases, typically with almost homogeneous cloud coverage, in which it is quite difficult to identify useful features.

A "feature" in these measurements constitutes a small cloud fragment or blob, an edge of a larger cloud, or any well-defined geometrical shape that can be tracked. The specific point on the feature to be tracked is chosen by the operator. For the current work we were typically dealing with features having a horizontal extent of the order of no more than a few hundred meters. The features commonly tracked in the satellite cloud images are much larger. For example, the clouds classified by Fujita et al. (1975) have horizontal dimensions ranging from 500 m to greater than 80 km

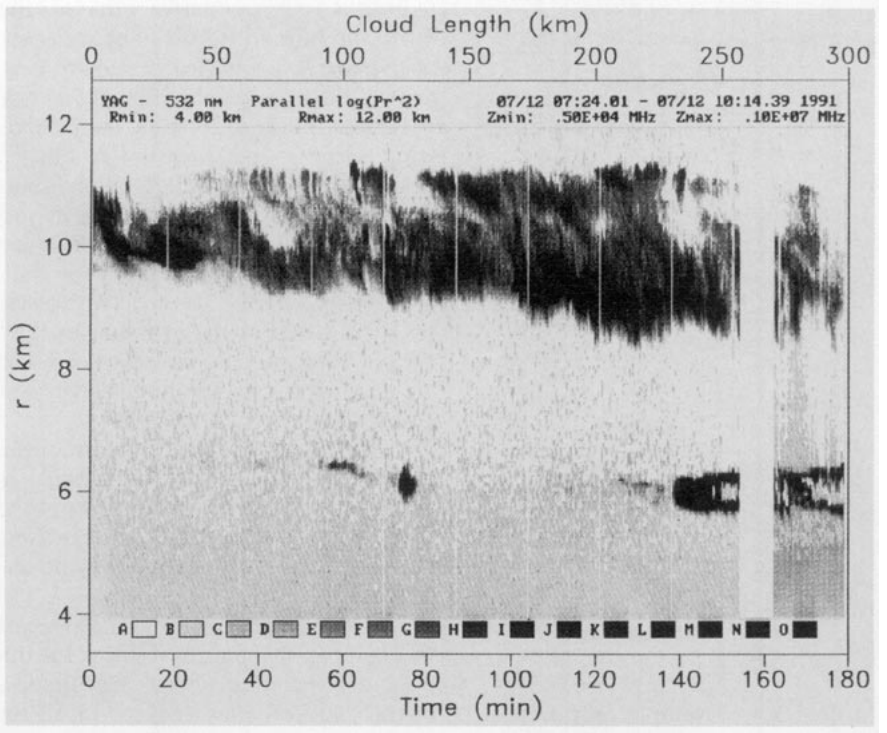

FIG. 1. Time–height gray-scale plot of lidar backscatter return from a relatively continuous cirrus layer. The top axis label is determined from the mean wind speed of the cirrus cloud layer at the 10-km altitude.

with a medium-size feature of about 15 km. Other measurements using ground-based and aerial photography for determining cloud displacements have also utilized large cloud features (Fujita et al. 1975; Hasler et al. 1977). Although the approach reported here employs the relatively fine structure of the clouds, it is possible to monitor cloud structures with horizontal dimensions in excess of 100 km by extending the duration of observation times.

For the data presented in this paper, the lidar has been operated with 75-m vertical range resolution. Although the lidar return signal provides a complete vertical profile of the cloud from bottom to top, there is still some ambiguity in assigning the exact height of the feature being tracked visually by the operator since there is no unique way of associating the feature with a particular altitude level within the profile. Lidar returns typically exhibit a sharp discontinuity (i.e., increase in signal) at the bottom of the cloud. The altitude of this cloud "bottom" is denoted as r_b. Somewhere within the volume of the cloud the lidar return signal reaches a maximum (peak) value. The altitude of this location is called r_p. The altitude of the cloud top, denoted as r_t, is the level at which the lidar signal level diminishes back down to the level of the return from the ambient atmosphere.

All three of these altitudes are determined and tracked automatically by the cloud-base algorithm described earlier (Pal et al. 1992). It is obvious that the height of the feature being tracked by the operator must lie between r_b and r_t but the exact location cannot be determined. In the analyses reported here, the location of the peak signal, r_p, was utilized as the altitude of the observed feature. Since this is the level within the cloud at which it has the greatest optical density, it should correlate closely with the location of the visual discontinuities defining the observable features.

It is recognized that the uncertainty in the altitude location of the feature will translate directly into an equivalent uncertainty in the derived wind speed. In choosing r_p we are confident that the uncertainty introduced is small. Statistical analysis of the large dataset of lidar cloud measurements available shows that the separation in altitude between r_p and r_b is typically less than 10% of r_b for all clouds above about the 2-km altitude. Thus, the uncertainty in the wind speed for these clouds should be even less than this value. For lower clouds the uncertainty increases, and for this reason no results have been included for altitudes below 2 km. In the remainder of this paper the designation r has been used for the height r_p of the tracked feature.

3. Measurements

As a part of the data retrieval and analysis procedures, a false color time–height plot of the lidar return

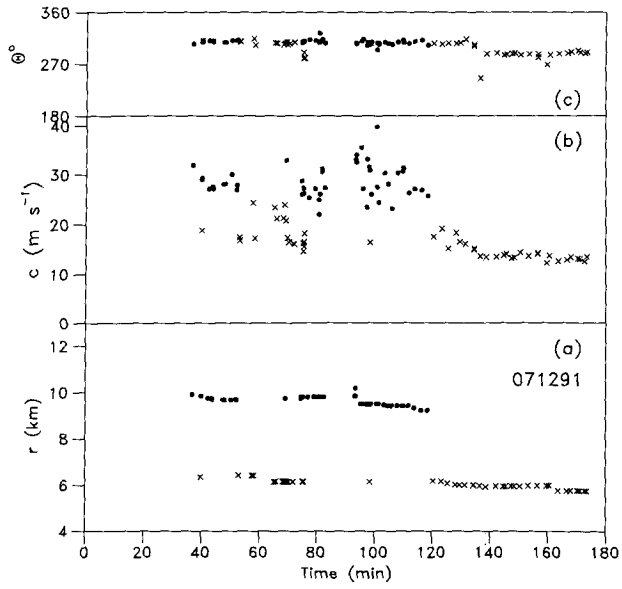

FIG. 2. Time variation of cloud height r, wind speed c, and direction θ for the data of Fig. 1.

signals is generated. In Fig. 1 a sample gray-scale reproduction of such a plot is shown. A 16-level gray scale is used to represent the logarithm of range-corrected lidar signal strength at each location.

In this figure is shown a time period of about 3 h and an altitude range from 4 to 12 km. This dataset shows two cloud layers. The upper, between about 9 and 11 km, is a relatively inhomogeneous but continuous layer of cirrus. The lower, at about 6-km altitude, is quite broken. Along the top of the figure is shown a horizontal distance scale derived from the measured mean speed of the upper-cloud layer. This information on the geometrical extent of the cloud is of assistance in matching the portion of the cloud probed by the lidar with the corresponding satellite image.

When dealing with multilevel clouds it can sometimes be difficult for the operator to associate the chosen feature with a particular layer. We have found that in general the different layers move with distinctly different velocities and that in most instances there are sufficient breaks in the layers to enable them to be differentiated without too much difficulty. Also the appearance of a feature is generally different in the different cloud layers. However, difficulties do arise when the lower layer is continuous and of sufficient density to obscure any upper layers. In this situation data are only obtainable at the lower altitudes.

Figure 2 shows wind data derived from Fig. 1. Figure 2a shows the time series of the altitude r of the clouds. The r values were obtained by averaging the altitude data over the time duration of 10 min or less in which the particular feature was tracked. Since the cloud was quite variable in structure as seen in Fig. 1, this averaging does provide some smoothing and was necessary to obtain a representative value for the cloud altitude during the time interval. The well-defined separation of the two levels is clearly shown as is the downward drift of the average cloud height as time progressed.

Figures 2b and 2c show, respectively, the derived wind speed c and direction θ. The data for the two levels are shown with different symbols. It is apparent that the two layers are traveling in very similar directions but with a considerably different speed. Simple summation of the data gives for the lower layer an average speed $\bar{c}$ of 16.0 m s^{-1} with a standard deviation of 3.1 m s^{-1}. For the upper layer the values are 28.7 m s^{-1} with a standard deviation of 3.4 m s^{-1}. The mean wind direction for the upper layer is $\bar{\theta} = 308° \pm 4°$, and for the lower, $294° \pm 14°$.

This averaging is not really an optimal way to treat the data since it is clear from Fig. 1 that the altitude of each layer is changing throughout the measurement. As a result the deviations from the average include this variation and are thus not indicative of inaccuracies of the measurement process.

Another useful form of data presentation is shown in Fig. 3. In this figure we show for the dataset of Fig. 2 the derived cloud speed as a function of the altitude of the feature being tracked. In all there are 48 data points shown for each layer. The format of Fig. 3 shows quite clearly the trend of the altitude dependence of the wind speed. It is seen from Fig. 3 that the increase of speed with altitude is seen within each layer although

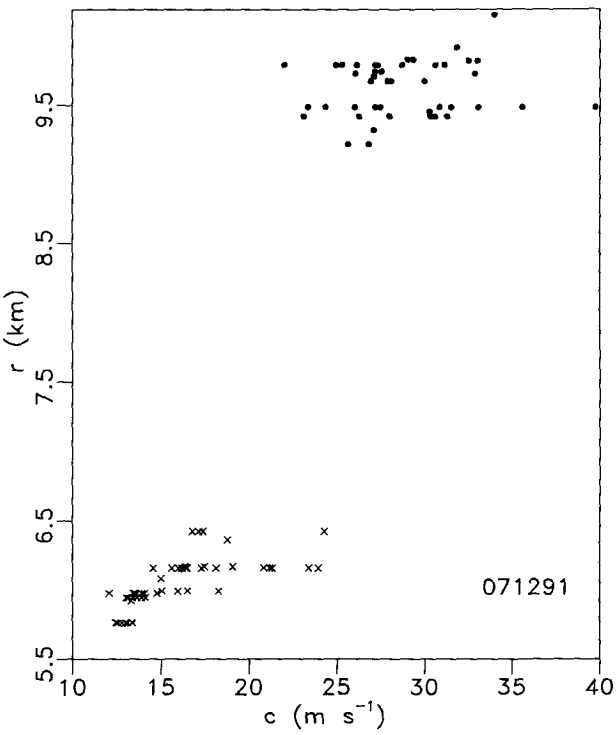

FIG. 3. The height variation of cloud velocity c for the data of Fig. 2.

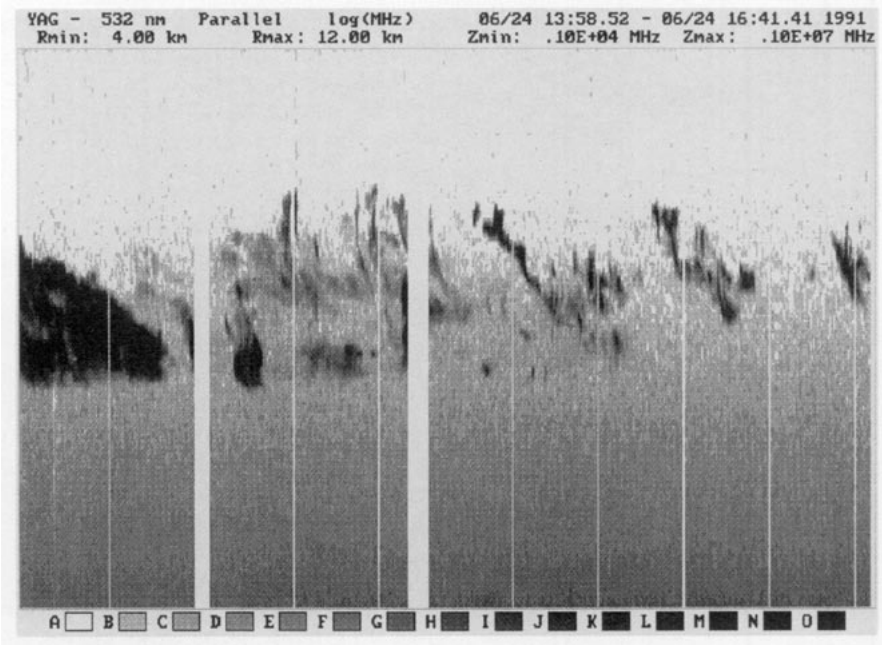

FIG. 4. Time–height plot of a broken cloud layer on 24 June 1991. Axes as in Fig. 1.

less so in the upper layer. Also, even with a relatively limited cloud vertical extent, considerable information on the wind profile is available. The scatter in the data arises from a combination of the fine-structure variability of the wind field and the scatter in the measurement method.

Wind measurements by Hasler et al. (1977) employing in situ aircraft and cloud motion detection from a geostationary satellite provide a comparison between the mean wind of the layer and the wind speeds at the cloud base, midcloud, and cloud-top levels. From the track lengths of 0.5–2.2 h used in their measurements they concluded that for tropical oceanic low-level cumulus as well as for high-level cirrus there was little difference in wind speeds at these three levels in a cloud. Our measurements with the finer resolution of the lidar profile often show well-defined height variation of cloud speed.

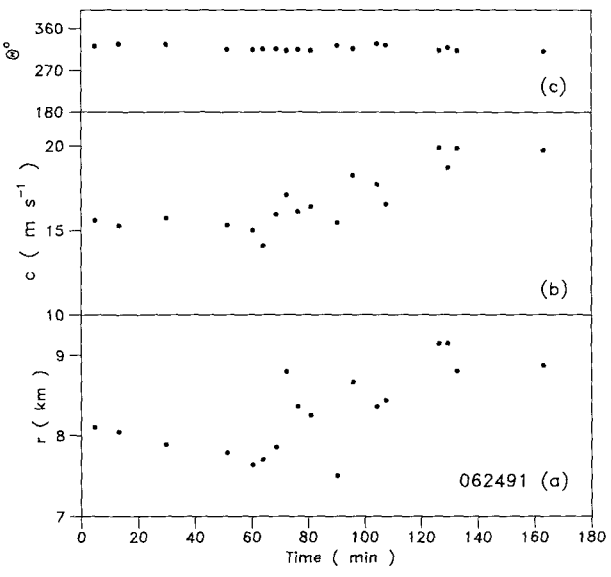

FIG. 5. Time record of r, c, and θ values from the data of Fig. 4.

As further indication of the ability to obtain information on the vertical wind profile, the data of Figs. 4–6 are shown. In this case a patchy cloud layer was found at altitudes between about 7.5 and 9 km. The gray-scale image is shown in Fig. 4 using the same time–height range as in Fig. 1. The time series for the altitude, wind speed, and direction are shown in Fig. 5. If we calculate a mean wind speed from this case we obtain a value of 16.8 ± 1.8 m s^{-1}. However, from the display in Fig. 5 it is clear that the speed is increasing appreciably with altitude.

This is shown more directly in Fig. 6 where plots for both the wind speed and direction are shown as a function of height. On the left of the figure are shown the raw data taken from Fig. 5. On the right a five-point running mean has been applied to provide some smoothing to the data. The increase of wind speed with height is clearly seen in both the raw and smoothed data. Shown in Figs. 6a and 6b are the best straight-line fits to the data. The straight-line fit for the raw data ($r = 0.27c + 3.8$) explains about 80% of the residuals about the mean, and the smoothed data ($r = 0.31c + 3.2$) about 96% about the mean. The corresponding linear correlation coefficients are 0.895 and 0.980, respectively.

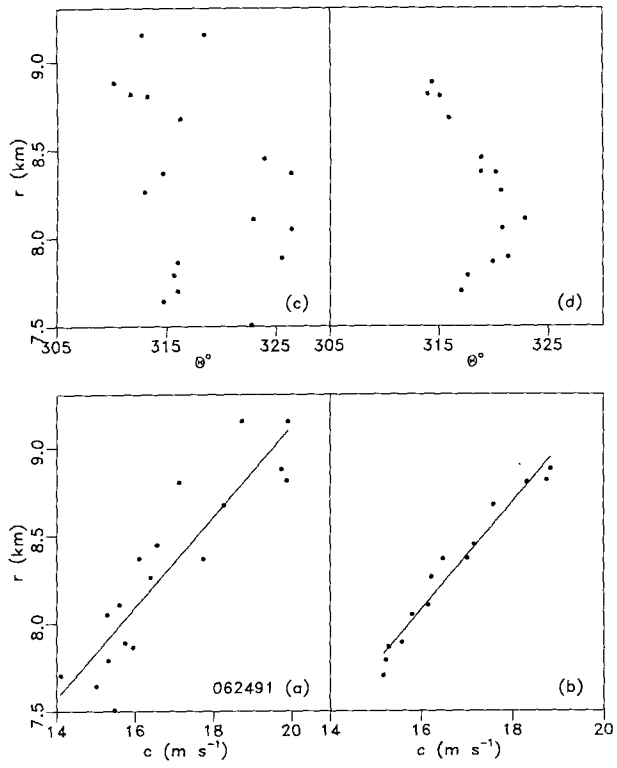

FIG. 6. Height variation of wind velocity c and direction θ for the data of Fig. 4. Plots are shown for raw data, (a) and (c), and with five-point smoothing, (b) and (d).

The behavior of the wind direction shown in Figs. 6c ($\bar{\theta} = 317.8° \pm 5.4°$) and 6d ($318.4° \pm 2.8°$) is also interesting. Although the scatter is large, there is an indication of a change in the wind direction with height.

Another interesting case is shown in the gray-scale display of Fig. 7. In this plot the vertical scale covers the height range from 1 to 12 km. In this example a cloud layer that is initially at an altitude of about 8 km descends steadily over the 3-h observation time to an altitude of about 2 km. In this figure the cloud top is quite realistically exhibited as is obvious from the right-hand side of the figure where lidar pulse penetration through the lower layer reveals another layer higher up. This was a rather difficult dataset to deal with because the continuity of the dense cloud greatly reduced the contrast on the video image. Even with the optimum video contrast settings the majority of features were trackable only for short intervals and this introduced additional uncertainty in the determination of the displacement coordinates. However, it was possible to obtain 46 wind measurements over the 2.5-h time interval. The aerosol features in the lower atmosphere are clearly seen in Fig. 7. Also apparent is the obscuration of the main cloud by a low-level cloud patch in the center of the figure.

In Fig. 8 both the raw and the smoothed speed and direction data are shown as in Fig. 6. The decrease of wind speed from 21 to 5 m s^{-1} with decreasing altitude over the entire range from 8 to 2 km is clearly shown. In Fig. 8 the linear fit to the raw data ($r = 0.31c + 1.03$) and the smoothed data ($r = 0.35c + 0.42$) explain, respectively, 84% and 98% of the residuals about the mean with correlation coefficients of 0.919 and 0.983. The lidar-derived low-altitude values are consistent with the measured surface wind speeds of 5.3, 4.7, and 4.2 m s^{-1} recorded from the local weather office at the start, middle, and end, respectively, of the 2.5-h measurement run. The mean of these is shown by the diamond symbol in Figs. 8a and 8b.

The wind direction in Figs. 8c (raw data) and 8d (five-point smoothing) with a mean value of $\bar{\theta} = 290.3° \pm 16.4°$ shows a larger range of values (between the extremes of 250° and 315°) compared to the other cases discussed here. Some altitude-dependent features in the wind direction are apparent. The analysis of cirrus and altostratus clouds has shown that a variation in the wind vector with height within a cloud layer is a frequent occurrence.

In Fig. 9 we illustrate this behavior for the data of Fig. 8 by plotting the wind vectors measured at each height. In Fig. 9 we show these vectors (**c**) displaced in the vertical direction plotted from a common vertical height axis. The zonal (**u**) and meridional (**v**) components are shown on the other two axes. The tips of the vectors have been joined with a solid line to show the altitude sequence more clearly.

4. Comparison of lidar and rawinsonde data

To date there has been no opportunity for a comprehensive lidar–rawinsonde measurement program. However, on a number of occasions for ECLIPS I data some sonde data were available for comparison with the lidar-derived wind information. The sondes were launched by the Canadian Atmospheric Environment Service from a site about 1 km from the lidar. All launches were made between about 1100 and 1230 LST while the ECLIPS lidar measurements were synchronized with the satellite overpasses. As a result for much of the lidar data the time differences were too great to permit meaningful comparisons to be undertaken.

In Fig. 10 comparisons are shown for seven different occasions during September, October, and November of 1989. The times shown in the figure are the beginning of the lidar 3-h run (L) and the launch time of the rawinsonde (R). In the figure the wind speed is shown on the left and the wind direction on the right. The lidar measurements are the solid circles and the sonde measurements are the open circles.

In comparing the two datasets in the figure it must be remembered that the measurements are being made on different spatial volumes of the atmosphere since the rawinsonde will in general be drifting at some distance from the lidar. In spite of this difference, the obtained values compare quite well. The scarcity of the sonde data points makes it difficult to ascertain the

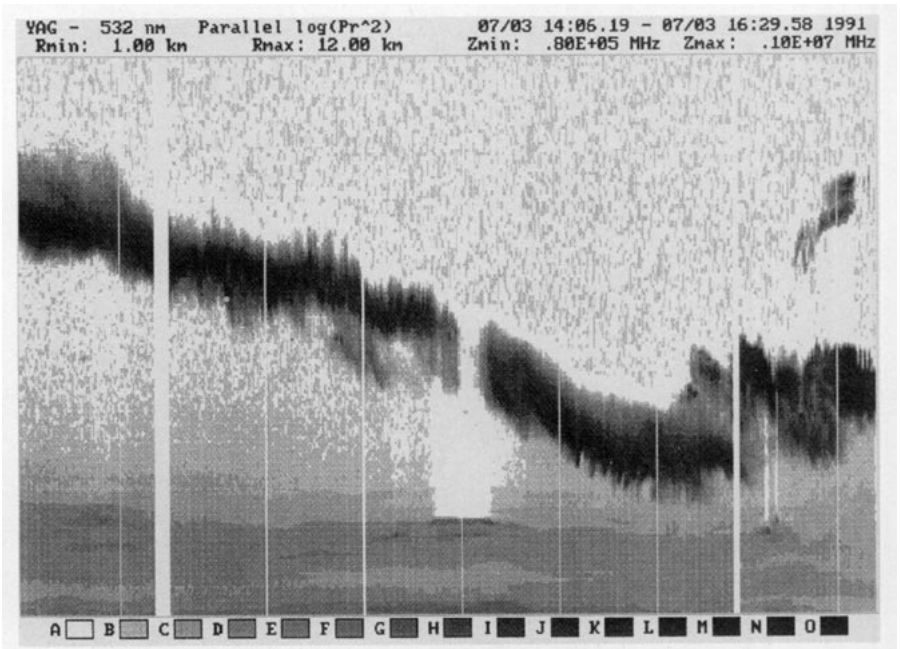

FIG. 7. Time–height plot for a cloud layer dropping in height with time. Vertical range is from 1 to 12 km.

scatter in these measurements compared to the much greater number of lidar measurements in a given region.

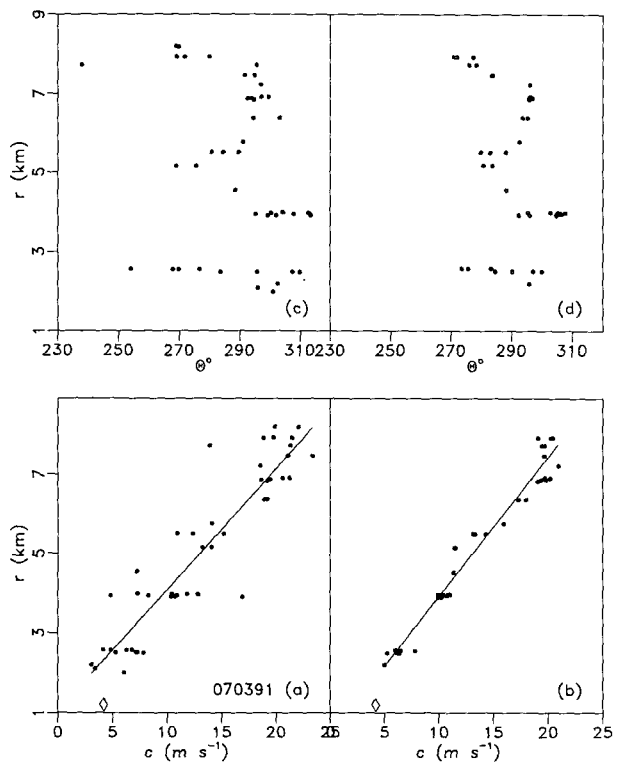

FIG. 8. Height variation of c and θ for the data of Fig. 7 plotted as in Fig. 6. The diamond symbol at the bottom indicates the measured mean surface wind speed during the lidar measurement.

On several occasions the sondes have provided wind data at the same altitude as the clouds (e.g., in Figs. 10a–c and 10g). In these instances the correspondence is extremely good with the measurements of both the speed and direction matching to within the scatter of the data. Unfortunately the rawinsonde dataset was very sparce and the opportunity for a more complete comparison was not available.

Bauer (1976) has compared satellite cloud-motion wind values with rawinsonde wind measurements and

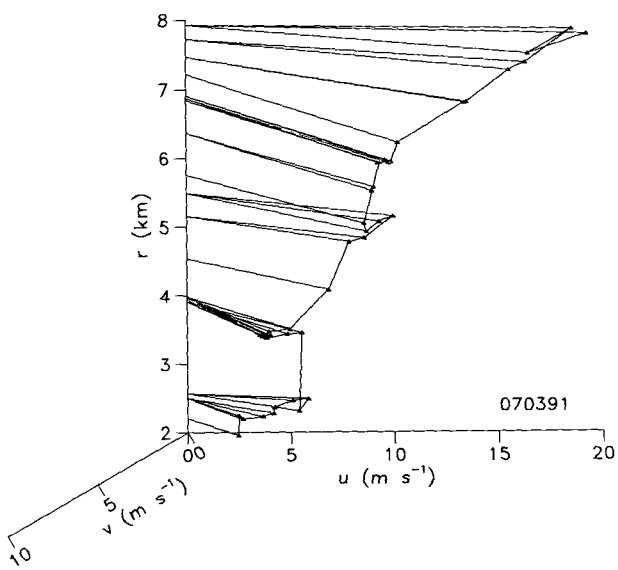

FIG. 9. Three-dimensional plot of the wind vectors for the data of Fig. 8; **u** is the zonal component, and **v** the meridional.

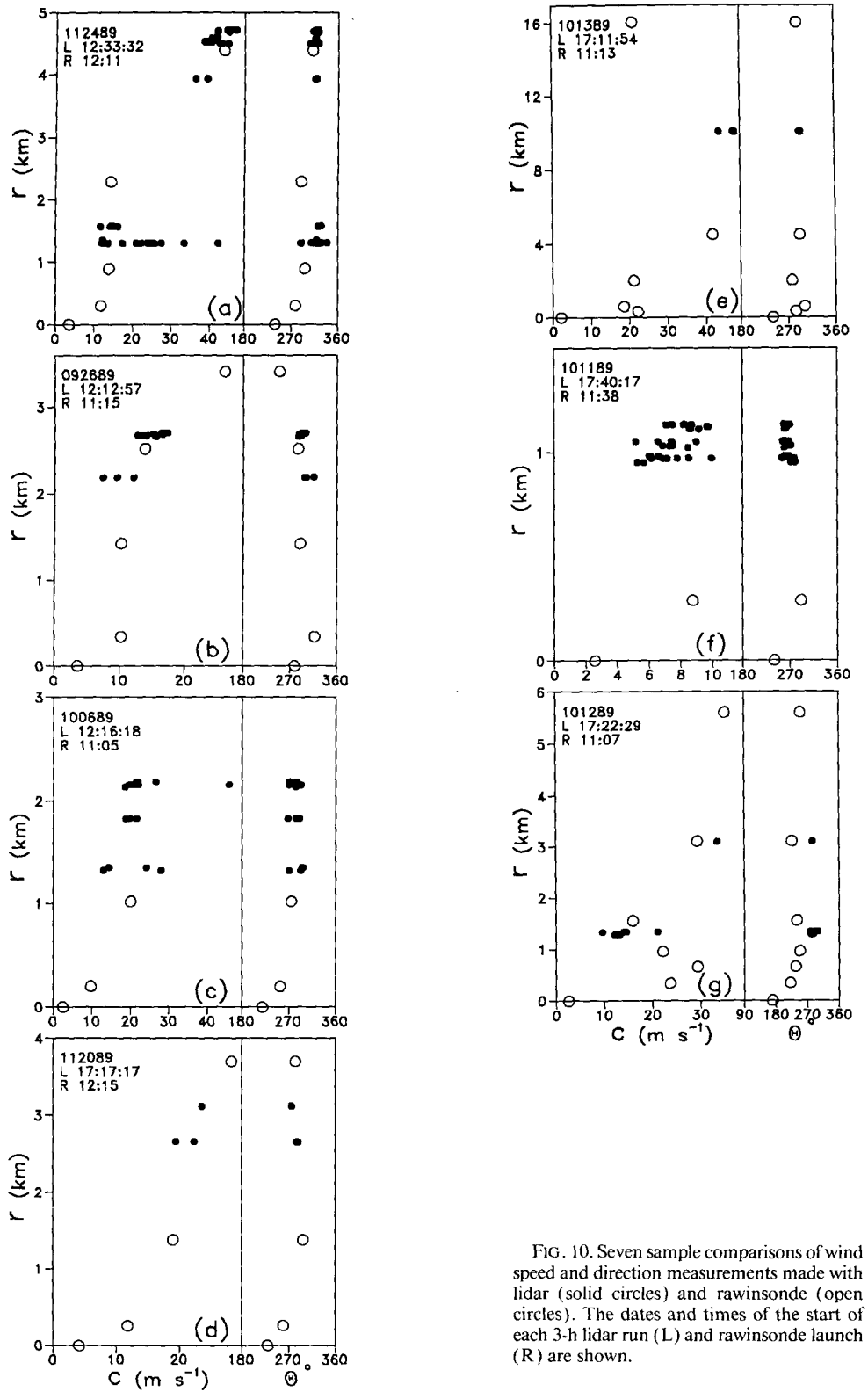

FIG. 10. Seven sample comparisons of wind speed and direction measurements made with lidar (solid circles) and rawinsonde (open circles). The dates and times of the start of each 3-h lidar run (L) and rawinsonde launch (R) are shown.

reports good correspondence between the two. His comparisons involved vertical and horizontal interpolation between winds reported from two or three rawinsondes within a radius of 660 km. Thus, his measurements suffer from the same difficulties of comparison as those shown in Fig. 10 since in neither case is it possible to sample identical spatial regions.

Rawinsonde wind measurements are typically derived from three-dimensional sonde displacements of many hundreds of meters. As a result the sonde data represent averages that will not display much of the fine structure of the wind field. The lidar cloud measurements, however, will show much of the detailed wind variability because of their inherently greater vertical resolution. This difference in the data is evident in Fig. 10. Since a lidar wind measurement can be made in times as short as a few minutes it is also possible to separate the temporal and spatial variabilities in the wind field.

5. Discussion

This investigation has shown that lidar cloud-tracked wind measurements are quite feasible and that quantitative data can be obtained. The standard deviations of our mean wind values, for example, are similar to those given by Fujita et al. (1975) and others. In fact the lidar information appears to be at least as good as the sonde measurements and demonstrates good potential for deriving additional information on some of the fine-structure features of the wind field.

Existing methods for wind measurements from cloud displacement require improved accuracy in cloud-height determination. The "height ambiguity" (Hubert 1969) is small in lidar measurements even for high cirrus, which otherwise pose considerable problems in wind measurements. For the thin layers best used for satellite wind studies, the lidar height uncertainty is negligible. As pointed out earlier, it is felt that the main cause of standard deviations in the current measurements is the real variability of the cloud motions.

Presently, our height determination is automatic, while the cloud tracking and displacement recording is not. It is clear, however, that more sophisticated and automated methods can be implemented, such as the Man–Computer Interactive Data Access System (Smith 1975; Chatters and Suomi 1975), cloud image cross-correlation techniques (Leese et al. 1971; Bowen et al. 1979; Turner and Warren 1989); Schmetz 1991) and automated pattern recognition (Endlich and Wolf 1981).

The tracked features in the present lidar method are small-scale cloud irregularities that are ever present in clouds. These irregularities can provide good time resolution in the associated winds and as a result could provide new information on the spatial and temporal variability of wind. The major limitation with the lidar cloud data is the restricted cloud occurrence in the atmosphere. The daytime-only video operation of the current study can be extended to nighttime measurements with more sensitive video equipment. The technique, however, is relatively localized, unlike the global coverage possible with satellite cloud images. Since clouds are often sparse and on some occasions nonexistent, the lidar method cannot guarantee the full coverage needed for modern weather networks. It is clear, however, that the lidar data could provide an excellent complement to existing measurements. By incorporating some of the automated image analysis routines currently in use for the satellite measurements, the information could be derived with little difficulty for many existing lidar sites (Abo et al. 1990).

In addition to this stand-alone capability for wind measurements, the lidar data on the cloud-height profile can be used to improve the satellite cloud-tracked wind information. This aspect will be pursued at ISTS in the future analysis of the ECLIPS data.

Acknowledgments. This lidar work is part of the research program of the Institute for Space and Terrestrial Science, a Centre of Excellence supported under the Ontario Premier's Council Technology Fund. This project is also supported by the Atmospheric Environment Service (AES) of Canada and the Natural Sciences and Engineering Research Council of Canada. The authors express their appreciation to the other members of the lidar group who contributed to this program, and to Mr. Gerald Klein of the AES for providing the rawinsonde data.

REFERENCES

Abo, M., C. Nagasawa, and O. Uchino, 1990: Remote wind velocity measurement using cloud motion detected by an RM-CW lidar and a CCD camera. *Rev. Laser Eng.*, **18,** 341–347.

Bauer, K. G., 1976: A comparison of cloud motion winds with coinciding radiosonde winds. *Mon. Wea. Rev.*, **104,** 922–931.

Bowen, R. A., L. Fusco, J. Morgan, and K. O. Roska, 1979: Operational production of cloud motion vectors (satellite winds) from METEOSAT image data: Use of data from meteorological satellites. *ESA,* **SP-143,** 65–75.

Carswell, A. I., S. R. Pal, W. Steinbrecht, J. A. Whiteway, A. Ulitsky, and T. Y. Wang, 1991: Lidar measurements of the middle atmosphere. *Can. J. Phys.*, **69,** 1076–1086.

Chatters, G. C., and V. E. Suomi, 1975: The applications of McIDAS. *IEEE Trans. Geosci. Electron.*, **GE-13,** 137–146.

Endlich, R. M., and D. E. Wolf, 1981: Automatic cloud tracking applied to GOES and METEOSAT observations. *J. Appl. Meteor.*, **20,** 309–319.

Fujita, T. T., E. W. Pearl, and W. E. Shenk, 1975: Satellite-tracked cumulus velocities. *J. Appl. Meteor.*, **14,** 407–413.

Fritz, S., and J. S. Winston, 1962: Synoptic use of radiation measurements from satellite TIROS-II. *Mon. Wea. Rev.*, **90,** 1–9.

Hasler, A. F., 1981: Stereographic observations from geosynchronous satellites: An important new tool for the atmospheric sciences. *Bull. Amer. Meteor. Soc.*, **62,** 194–212.

——, W. E. Shenk, and W. C. Skillman, 1977: Wind estimates from cloud motions: Results from phases I, II and III of an in situ aircraft verification experiment. *J. Appl. Meteor.*, **16,** 812–815.

Hubert, L., 1969: Estimating winds from satellite pictures. Part I—Accuracy of wind estimates from geostationary satellites. Appendix K to World Weather Watch Planning Report No. 30, WMO, 3 pp. [Available from Dr. L. Hubert, National Environmental Satellite Service, NOAA, Washington, D.C.]

Leese, J. A., C. S. Novak, and B. B. Clark, 1971: An automated technique for obtaining cloud motion from geosynchronous satellite data using cross correlation. *J. Appl. Meteor.*, **10,** 118–132.

Menzel, W. P., W. L. Smith, and T. R. Stewart, 1983: Improved cloud motion wind vector and altitude assignment using VAS. *J. Climate Appl. Meteor.*, **22,** 377–384.

Merrill, R. T., 1989, Advances in the automated production of wind estimates from geostationary satellite imaging. *Proc. Fourth Conf. on Satellite Meteorology,* San Diego, Amer. Meteor. Soc., 246–249.

——, W. P. Menzel, W. Baker, J. Lynch, and E. Legg, 1991: A report on the recent demonstration of NOAA's upgraded capability to derive cloud motion satellite winds. *Bull. Amer. Meteor. Soc.,* **72,** 372–376.

Mosher, F. R., 1976: Cloud height determination. COSPAR Proc. Symp. Meteorological Observations from Space: Their Contribution to the First GARP Clobal Experiment, NCAR, Boulder, CO, 201–204.

Pal, S. R., W. Steinbrecht, and A. I. Carswell, 1992: Automated method for lidar determination of cloud base height and vertical extent. *Appl. Opt.*, **31,** 1488–1494.

Piironen, A. K., and E. W. Eloranta, 1993: Wind profiling with the volume imaging lidar: A comparison with aircraft and balloon based measurements. Optical Remote Sensing of the Atmosphere Technical Digest, (Optical Society of America, Washington, DC., 1993), **5,** 240–243.

Platt, C. M. R., 1988: Experimental cloud lidar pilot study (ECLIPS), Report of the WCRP/CSIRO, Cloud Base Measurement Workshop, CSIRO, Division of Atmospheric Research, Mordialloc, Victoria, Australia. [Available from Dr. C. M. R. Platt, Division of Atmospheric Research, CSIRO, Private Bag No. 1, Mordialloc, Victoria, Australia, 3195.]

——, S. A. Young, A. Carswell, S. Pal, M. P. McCormick, D. Winker, M. Del Guasta, W. Eberhard, P. Flamant, B. Forgan, G. Gimmestad, M. Hardesty, H. Jager, S. Khmelevtsov, I. Kolev, Darren Lu, Y. Mizuno, K. Sassen, V. Shamanaev, L. Stefanutti, O. Uchino, U. Wandinger, C. Weitkamp, A. Ansmann, and C. Wooldridge, 1993: The Experimental Cloud Lidar Pilot Study (ECLIPS) for cloud-radiation applications. *Bull. Amer. Meteor. Soc.*, submitted.

Reynolds, D., and T. Vonder Haar, 1977: A bi-spectral method for cloud parameter determination. *Mon. Wea. Rev.*, **105,** 446–457.

Rutledge, G., E. Legg, and P. Menzel, 1991: Operational production of winds from cloud motions. *Palaeogeogr., Palaeoclim., Palaeoecol,* **90,** 141–150.

Sadler, J. C., and B. J. Kilonsky, 1985: Deriving surface winds from satellite observations of low-level cloud motions. *J. Climate Appl. Meteor.*, **24,** 758–769.

Schmetz, J., 1991: Cloud motion winds from METEOSAT: performance of an operational system. *Palaeogeogr., Palaeoclim., Palaeoecol.,* **90,** 151–156.

Smith, E., 1975: Man–computer interactive data access system. *IEEE Trans. Geosci. Electron.*, **GE-13,** 123–136.

Suchman, D., and D. W. Martin, 1976: Wind sets from SMS images: An assessment of quality for GATE. *J. Appl. Meteor.*, **15,** 1265–1278.

Turner, J., and D. E. Warren, 1989: Cloud track winds in the polar regions from sequences of AVHRR images. *Int. J. Remote Sens.*, **10,** 695–703.